

Optics Letters

Few-cycle, mJ-level, mid-wave infrared pulses generated via post-compression of a chirped pulse amplifier

Z. Alphonse Marra, 1,2 Yi Wu, 1 D Nicholas Belden, 1 and Zenghu Chang 1,2,* D

Received 29 March 2024; revised 2 May 2024; accepted 5 May 2024; posted 8 May 2024; published 29 May 2024

Few-cycle pulses were generated by passing a beam from a cryogenically cooled Fe:ZnSe chirped-pulse amplifier (CPA) at a repetition rate of 400 Hz through a gas-filled hollow core fiber (HCF) followed by dispersion-compensating bulk CaF2. The krypton-filled fiber at 370 kPa yielded 1.14-mJ, 42-fs pulses centered at 4.07 μm , while the oxygen-filled fiber at 310 kPa delivered 0.78-mJ, 39-fs pulses spanning from 3 to 5.5 μm . This work is a step toward a high repetition rate mid-wave infrared driver of isolated attosecond keV x-ray pulses. © 2024 Optica Publishing Group

https://doi.org/10.1364/OL.524212

Carrier-envelope phase (CEP)-stabilized, few-cycle lasers with 1 kHz or higher repetition rates in the near-infrared (NIR) region have reached a mature stage of technological development for attosecond science applications [1]. The endeavor to expand this technology deeper into the infrared spectrum is currently gaining significant momentum. Several key phenomena in strong field physics motivate the push for longer wavelength sources. Important wavelength scaling laws apply to the cutoff of highharmonic generation (HHG) [2], the critical power of relativistic self-focusing [3], the critical power for Kerr-driven self-focusing [4], and THz generation efficiency [5] among others [6]. Central to this research, the single-atom cutoff photon energy of HHG scales approximately as the square of the driving laser center wavelength. The HHG cutoff energy also scales approximately linearly with laser intensity [7], therefore demanding driving lasers with short pulse durations, high pulse energies, and good beam quality. Indeed, for isolated attosecond pulse generation, the requirements include near-single-optical-cycle pulse duration, CEP stability, and peak intensities exceeding 10¹⁴ W/cm²

Chirped pulse amplification based on an Fe:ZnSe gain medium with seeding by an optical parametric amplifier has been demonstrated to produce high-energy pulses in the midwave infrared (MWIR) region [9–11], but such pulses are far from few-cycle duration. Fe:ZnSe-based chirped-pulse amplifier (CPA) pulses may be further compressed by taking advantage of the adjustable nonlinear refractive index, sustained high intensities, and the long interaction length afforded by a pressurized

hollow core fiber (HCF). The application of HCFs for nonlinear pulse compression of NIR lasers has been historically successful [12,13], yet the adoption of this technique with MWIR sources has been limited. In one recent experiment, researchers sent the coherent beam combination of two MWIR optical parametric chirped-pulse amplifiers (OPCPA) through a HCF filled with krypton gas to yield 2.7-mJ, 22.9-fs, 20-Hz pulses centered at 4 μm [14]. While this approach is potentially scalable to an arbitrary number of OPCPA channels, each OPCPA channel is complex, requiring precise alignment and synchronization. A similar OPCPA-based system generated 2.6-mJ, 21.5-fs, 100-Hz pulses without the use of coherent beam combination via a krypton-filled HCF [15]. Both systems achieved impressive peak powers over 100 GW, but overall conversion efficiencies from the Nd:YAG pump lasers to the few-cycle MWIR pulses were low at around 1%. Notably, HCF compression was also accomplished at 3.2 µm providing 2.5-mJ, 22-fs pulses [16].

This Letter presents the continuation of development of a 400-Hz, 4.07- μ m, cryogenically cooled Fe:ZnSe CPA [10], with improvements to the amplifier itself plus an added stage of nonlinear pulse compression via a gas-filled hollow core fiber. The hollow core fiber proved to reduce the pulse duration to ~40 fs and to increase the peak power of the source by a factor of up to 2.25.

Suppression of amplified spontaneous emission in Fe:ZnSe CPA. Since a previous publication [10], the repetition rate of the CPA has been increased from 333 to 400 Hz, and four additional passes of the amplifier have been added. Figure 1 shows an optical layout of the entire system including the seed generation system, stretcher, amplifier, compressor, and HCF nonlinear compression stage.

As passes are increased from eight to twelve, the effect of amplified spontaneous emission (ASE) increases. The time scale of the ASE buildup is tens of microseconds and is caused by the $\sim\!100\text{-}\mu\text{s}$ pump lasers for the cryogenically cooled Fe:ZnSe crystals. Therefore, an optical chopper (Stanford Research Systems) was added between the fifth and sixth passes to interrupt the buildup of such energy-depleting ASE. Focusing the beam to a diameter of $\sim\!50\mu\text{m}$ at the plane of the 4-in.-diameter chopper blades running at a shaft frequency of 200 Hz gives a temporal edge of $\sim\!1~\mu\text{s}$. With a 30-slot blade, the timing jitter of

¹Institute for the Frontier of Attosecond Science and Technology, The College of Optics and Photonics (CREOL) and Department of Physics, University of Central Florida, Orlando, Florida 32816, USA

²Laboratory for Infrared-driven Intense-field Science, Department of Physics, University of Ottawa, Ottawa, Ontario K1N 7N9, Canada *zchang@uottawa.ca

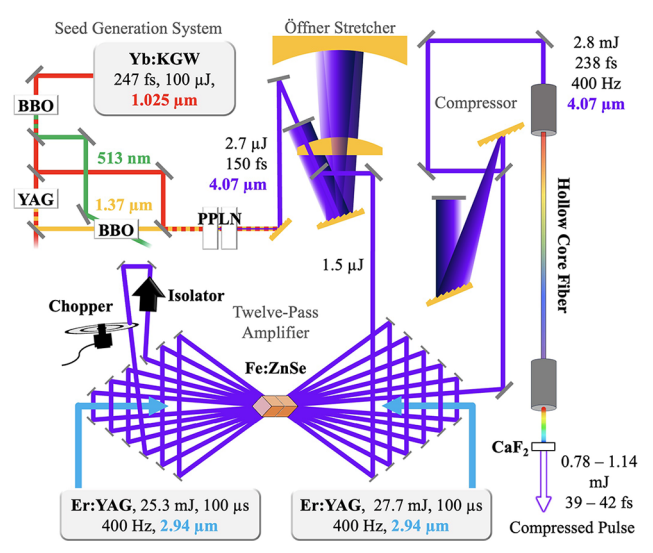


Fig. 1. CPA system begins with a Yb:KGW laser, which pumps a two-stage optical parametric amplifier producing seed pulses. From there, pulses are stretched in an Öffner-style stretcher followed by a 12-pass amplifier. A chopper and an isolator are placed between the fifth and sixth passes to interrupt ASE, a parasitic effect that precedes the seed pulse. After amplification, pulses are compressed in a grating pair. Finally, pulses are sent into a gas-filled HCF followed by dispersion-compensating bulk CaF₂.

the chopper is estimated to be 0.46 μs RMS. In principle, the chopper in this configuration may support repetition rates up to 6 kHz. The ASE is effectively interrupted until the seed pulse passes through the amplifier. After the seed pulse, excited state population has largely been depleted, and the pump lasers are no longer active; therefore, ASE following the seed pulse is not observed. To further prevent ASE, a Faraday isolator was also placed between passes five and six. Figure 2 shows the spectrum of the amplifier output with the chopper active and with the chopper stopped in an open position. The figure shows that ASE can be effectively suppressed by the chopper and isolator. It is worth noting that a chopper scheme cannot be implemented for Fe:ZnSe operating at room temperature for which the duration of the pump lasers is less than 1 μs . A Pockels cell, which is not easily available for 4 μm , would be needed for such lasers.

At a repetition rate of 400 Hz, the pulse energy is 4.33 mJ directly after the amplifier, before compression. After compression and directing optics, 2.88 mJ reaches the input of the HCF. While purging the amplifier system with nitrogen gas to reduce CO₂ absorption at 4.2 µm was tested, it was deemed unnecessary and was not implemented. The duration of this input pulse was measured to be 238 fs at the full width at half maximum (FWHM) by a frequency-resolved optical gating (FROG) system, as shown in Fig. 3. For the FROG, a beam splitter on a 0.43-mm CaF₂ substrate equally divided the beam with one arm being temporally scanned during the measurement. The beams were then crossed at an angle of $\sim 6^{\circ}$ and focused onto a 30-µm-thick GaSe crystal by a 50-mm focal length off-axis parabolic mirror. An InGaAs spectrometer (Spectral Evolution) with a sensitivity range of 1.1 to 2.6 µm captured the spectra of second-harmonic light generated at an angle between the two fundamental pulses at varying delay steps. A noncollinear FROG geometry is necessary when the bandwidth of the fundamental

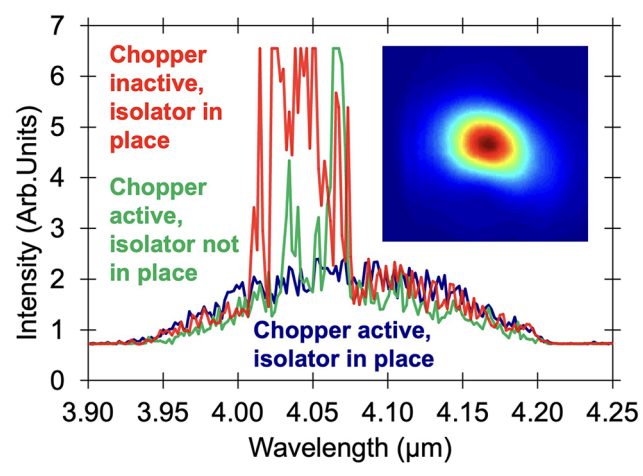


Fig. 2. CPA output spectra different configurations of the chopper and isola. The beam profile, measured using a pyroelectric camera from Ophir-Spiricon, before passing through the HCF is also shown. Pulses are centered at $4.07~\mu m$.

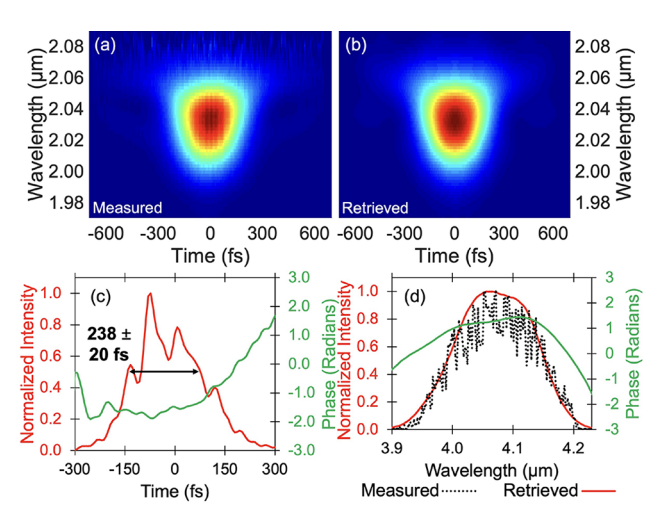


Fig. 3. Temporal characterization of the CPA pulses before nonlinear compression via HCF. Measured (a) and retrieved (b) FROG traces. Retrieved pulse shape with temporal phase (c). Measured and retrieved spectra with spectral phase (d). FROG error is 0.00255.

pulse is greater than one octave. This is to prevent the fundamental frequency and the sum frequency from interfering with each other. Variation in the results of the FROG retrieval algorithm (FROG 3.2.2 from Swamp Optics, LLC) led to the inclusion of a calculation of uncertainty in the pulse duration, which may be expressed as a standard deviation of the distribution of retrieval outputs. For the CPA, the standard deviation was 20 fs.

HCF pulse compression. The HCF (Few-Cycle Inc.) was filled with either krypton or oxygen gas at varying pressures up to $\sim\!350$ kPa to maximize spectral broadening. Its diameter was 1 mm, its length was 2.9 m, and it was not differentially pumped, meaning the pressure was maintained constant at both ends of the fiber. Depending on the gas type and gas pressure inside the HCF, transmission was recorded to be between 48 and 59%. Oxygen tended to be less transmissive than krypton. This may be partially due to the Raman process in the oxygen molecular gas and the lack of suitable antireflective coatings on the window that accommodate the broader spectral bandwidth.

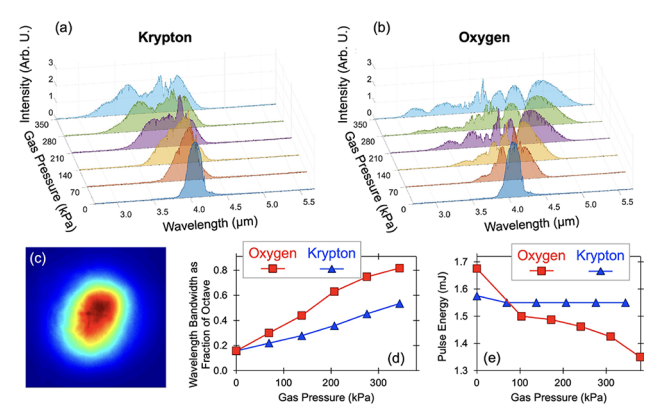


Fig. 4. Measured spectra versus HCF gas pressure for krypton-filled HCF (a) and oxygen-filled HCF (b). Beam profile after HCF transmission (c). Wavelength bandwidth as a fraction of an octave (d) and total pulse energy (e) versus gas pressure for both oxygen and krypton-filled HCFs.

In the case of the krypton-filled HCF, self-phase modulation (SPM) caused characteristic symmetric broadening about the center wavelength, as Fig. 4(a) shows. SPM generally applies a positive chirp to the pulse, which can be well compensated with a negative dispersion material such as CaF₂. With oxygen, Raman scattering caused by molecular vibrations of oxygen molecules led to a redshift in the spectrum. Figure 4(b) shows the broadening of the spectrum after the oxygen-filled HCF, for which SPM and Raman scattering broaden the spectrum to nearly an octave. To compensate for the added dispersion caused by SPM and Raman scattering, bulk CaF₂ was added after the HCF output. In the case of the 370-kPa krypton-filled HCF, 5.5 mm total of CaF₂ was used to minimize chirp, giving the shortest pulse duration. For oxygen at 310 kPa, 4 mm of CaF₂ total was used. The thickness of the FROG beam splitter was not accounted for as it was relatively thin.

The powermeter indicates 1.55-mJ and 1.39-mJ pulses after the 370-kPa krypton-filled HCF and the 310-kPa oxygen-filled HCF, respectively; however, some energy is in the pedestals of the pulses, as shown in Figs. 5(c) and 6(c). Integrating over just the shape of the main pulse in each case gives pulse energies of 1.14 mJ for krypton and 0.78 mJ for oxygen, values which are used for calculating peak power. Residual energy is in the pedestals of the pulses. For oxygen, a more complex spectral phase, which is less easily compensated by materials, is accumulated due to Raman scattering, causing less of the pulse energy to be under the principal pulse. As a result, the peak powers of the pulses were 25.5 GW for krypton and 18.8 GW for oxygen. Krypton yielded 42-fs FWHM pulses with a standard deviation of 2 fs, corresponding to 3.13 cycles at 4 µm. Oxygen yielded 39-fs FWHM pulses or 2.94 optical cycles with a standard deviation of 3 fs. Because the sensitivity of the InGaAs detector begins to drop at 2.5 µm and fully cuts off at 2.6 µm, the full range of the spectra in the oxygen FROG trace may be cut short, which suggests the pulse duration may be shorter than what was possible to record by this system. Based on the spectra measured, Fourier-transform-limited (FTL) pulse durations of 31 fs and 22 fs were calculated for krypton and oxygen, respectively. Implementing better chirp compensation schemes such as MWIR chirped mirrors and pulse shapers may lead to near-single-cycle pulses with mJ-level energy. Comparing the krypton results of this work to previous, comparable krypton

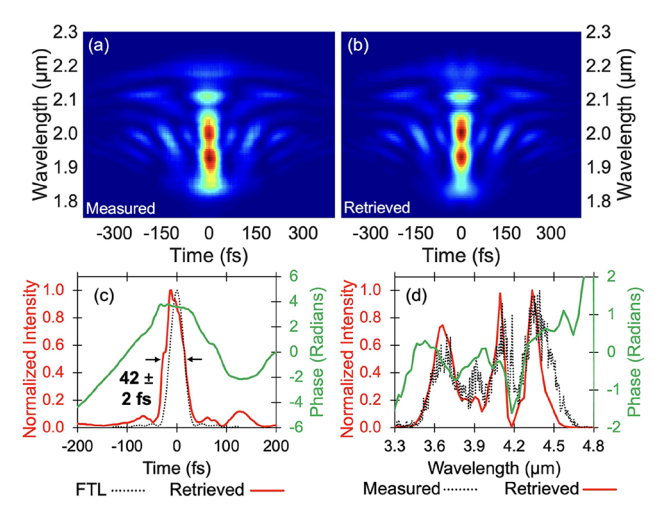


Fig. 5. Temporal characterization of the krypton-filled HCF pulses. Measured (a) and retrieved (b) FROG traces. FTL pulse shape based on the measured spectrum and retrieved pulse shape with temporal phase (c). Measured and retrieved spectra with spectral phase (d). FROG error is 0.00579.

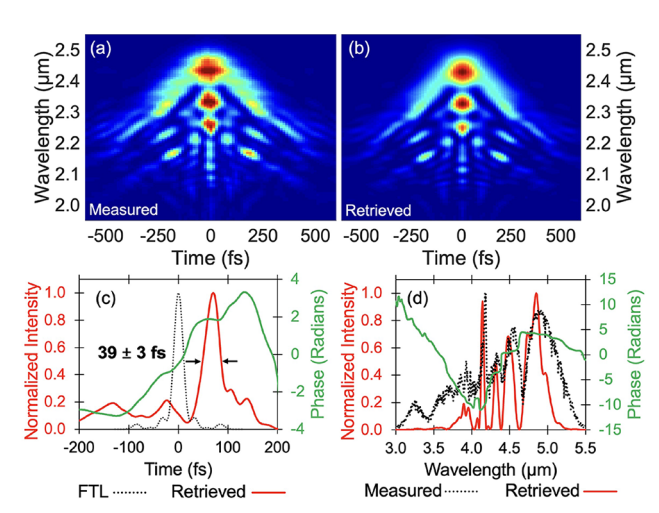


Fig. 6. Temporal characterization of the oxygen-filled HCF pulses. Measured (a) and retrieved (b) FROG traces. FTL pulse shape based on the measured spectrum and retrieved pulse shape with temporal phase (c). Measured and retrieved spectra with spectral phase (d). FROG error is 0.00639.

HCF experiments [14,15] demonstrates several key strengths to the approach of starting with a cryogenically cooled Fe:ZnSe CPA source. With a net pump pulse energy of 53 mJ from both Er:YAG lasers, a pump-to-few-cycle pulse efficiency of 2.15% for krypton was achieved. This is more than double what was achieved in the previous experiments. Moreover, the average power of this source was more than a factor of 2 greater due to its repetition rate being significantly higher, an attractive feature for many practical applications. For the krypton-filled HCF in this work, a compression factor of 5.71 was recorded, which is comparable to [14] (6.99) and [15] (4.88). However, the HCF method of compression is an improvement over using a krypton-filled gas cell, as shown when a similar 4.55-µm system was compressed to 62 fs with a compression factor of just 2.6 [11].

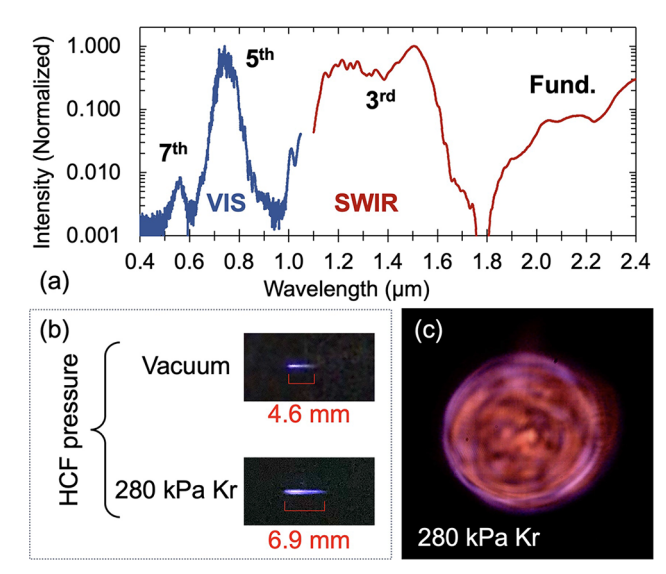


Fig. 7. (a) Harmonics spectra for 350-kPa Kr measured using a silicon-based (VIS) spectrometer (Ocean Insight) and an InGaAsbased (SWIR) spectrometer. (b) Side view of plasma ionization forming a filament in air after being focused via a 50-mm focal length off-axis parabolic mirror. (c) Color photo of the conical emission from the filament for 280-kPa Kr.

Lastly, the source was focused in air by a 50-mm focal length off-axis parabolic mirror to generate odd harmonics up to the seventh order (\sim 581 nm) indicating its potential for use in strong-field experimentation as shown in Fig. 7. The focused beam is estimated to have a peak intensity on the order of 10^{15} W/cm², which is expected to be sufficient for keV HHG. By imaging the filament on axis, a color photo may be taken showing the conical emission of the harmonics as shown in Fig. 7(c). Figure 7(b) shows a side view of the filament contrasting the HCF at vacuum and at 280 kPa krypton.

Conclusion. This work is both the first demonstration of fewcycle, MWIR pulses originating from a cryogenically cooled Fe:ZnSe CPA directed into a gas-filled HCF and the first published use of oxygen for broadening via HCF of a 4- μ m source. Compared to krypton, the HCF filled with oxygen resulted in a broader spectrum and a shorter FWHM pulse duration; however, much of the pulse energy lay outside of the principal pulse and was unable to be compensated with bulk CaF₂ leading to lower peak power. At 400 Hz, the repetition rate of this source is

greater than most comparable sources. Moreover, its pump laser energy conversion efficiency is significantly greater. The source employs commercially available, free-running Er:YAG lasers that are much simpler than the complex picosecond Nd:YAG amplifiers used in [14,15]. These Er:YAG lasers can be upgraded for greater pulse energy, allowing a simple method of scaling the CPA pulse energy leading to a greater compression factor through the HCF. CEP stability may be established in future updates to the CPA. The CEP of the seed pulses is potentially stable due to the difference frequency generation scheme. According to [15], the CEP of MWIR pulses was preserved through a Kr-filled HCF.

Funding. Air Force Office of Scientific Research (FA9550-20-1-0295); Canada Excellence Research Chairs, Government of Canada; National Defense Science and Engineering Graduate.

Acknowledgment. The authors thank Dr. Bruno Schmidt at Few-Cycle Inc. for the advice on the hollow core fiber installation and operation.

Disclosures. The authors declare no conflicts of interest.

Data availability. Data underlying the results presented in this paper are not publicly available at this time but may be obtained from the authors upon reasonable request.

REFERENCES

- 1. M. Chini, K. Zhao, and Z. Chang, Nat. Photonics 8, 178 (2014).
- 2. B. Shan and Z. Chang, Phys. Rev. A 65, 011804 (2001).
- F. Sohbatzadeh, M. Rabbani, and M. Ghalandari, Opt. Commun. 285, 3191 (2012).
- 4. A. Couairon and A. Mysyrowicz, Phys. Rep. 441, 47 (2007).
- I. A. Nikolaeva, D. E. Shipilo, N. A. Panov, et al., Photonics 9, 974 (2022).
- Z. Chang, L. Fang, V. Fedorov, et al., Adv. Opt. Photonics 14, 652 (2022).
- J. L. Krause, K. J. Schafer, and K. C. Kulander, Phys. Rev. Lett. 68, 3535 (1992).
- Z. Chang, P. B. Corkum, and S. R. Leone, J. Opt. Soc. Am. B 33, 1081 (2016).
- 9. A. Pushkin and F. Potemkin, Photonics 10, 1375 (2023).
- 10. Z. A. Marra, Y. Wu, F. Zhou, et al., Opt. Express 31, 13447 (2023).
- 11. E. Migal, A. Pushkin, N. Minaev, et al., Opt. Lett. 47, 985 (2022).
- 12. G. Fan, P. A. Carpeggiani, Z. Tao, et al., Opt. Lett. 46, 896 (2021).
- 13. M. Nisoli, S. D. Silvestri, O. Svelto, et al., Opt. Lett. 22, 522 (1997).
- 14. J. Qian, P. Wang, Y. Peng, et al., Photonics Res. 9, 477 (2021).
- 15. P. Wang, Y. Li, W. Li, et al., Opt. Lett. 43, 2197 (2018).
- 16. G. Fan, T. Balčiūnas, T. Kanai, et al., Optica 3, 1308 (2016).